Mechanism of the enhanced thermoelectric power in (111)-oriented *n*-type PbTe/$Pb_{1-x}Eu_xTe$ multiple quantum wells

T. Koga
Division of Engineering and Applied Sciences, Harvard University, Cambridge, Massachusetts 02138

T. C. Harman
Lincoln Laboratory, Massachusetts Institute of Technology, Lexington, Massachusetts 02420

S. B. Cronin and M. S. Dresselhaus
Department of Physics, Massachusetts Institute of Technology, Cambridge, Massachusetts 02139
(Received 30 June 1999)

A theoretical investigation of the recently observed enhanced thermoelectric power S in (111)-oriented *n*-type PbTe/$Pb_{1-x}Eu_xTe$ multiple-quantum-wells ($x \simeq 0.09$) has been carried out, including both longitudinal acoustic phonon deformation potential scattering and polar optical phonon scattering of the two-dimensionally confined electrons in the quantum wells. An enhancement in S is observed experimentally and predicted theoretically, despite the lifting of the conduction band valley degeneracy, and an excellent agreement between the experimental and theoretical results has been obtained over a wide temperature range (80–400 K). In the low temperature regime ($\sim$100 K), the polar optical phonons are found to be more effective in scattering carriers in the oblique L-point valleys than in scattering carriers in the longitudinal L-point valley, making the resulting S somewhat suppressed in this temperature regime. In the high temperature regime ($\geqslant$300 K), the polar optical phonon scattering generally contributes to increasing S due to the particular shape of the distribution function associated with it. It is emphasized that our theoretical model requires virtually no fitting parameters. The excellent agreement between the theoretical and experimental results suggests the validity of our model of enhanced thermoelectric figure of merit in two-dimensional structures and the reliability of the values of the parameters for the superlattice deduced from other independent measurements, such as Hall carrier concentrations and band energy gaps. [S0163-1829(99)07243-4]

I. INTRODUCTION

There has been considerable interest in the thermoelectric properties of low-dimensional systems, such as two-dimensional quantum wells[1–15] and one-dimensional quantum wires[16–20] since Hicks and Dresselhaus predicted that the thermoelectric figure of merit (ZT) for such low-dimensional systems should be substantially enhanced relative to the corresponding bulk materials as the size of the sample is reduced to the nm (or Å) range.[1,16] This idea was first demonstrated experimentally by Harman *et al.*[3] and Hicks *et al.*[4] using MBE grown (111)-oriented PbTe/$Pb_{1-x}Eu_xTe$ multiple-quantum-well (MQW) samples. The observed enhanced thermoelectric properties in this system was first interpreted in terms of the constant relaxation time approximation (CRTA), assuming various values for the ratio of the carrier mobilities between the longitudinal valley and the oblique valleys.[4,6] Recently, Broido and Reinecke performed calculations of thermoelectric transport coefficients for the (111) oriented PbTe MQWs at 300 K by solving the Boltzmann equation numerically, including both elastic and inelastic scattering mechanisms explicitly, but assuming a parabolic energy dispersion relation and using the approximation of isotropic constant energy surfaces. They pointed out that the Seebeck coefficient for the PbTe MQW samples should be largely suppressed due to the lifting of the valley degeneracy between the longitudinal and oblique valleys in (111)-oriented PbTe MQW samples.[12] However, this latter point was inconsistent with the observed enhancement in the thermoelectric power in the PbTe/$Pb_{1-x}Eu_xTe$ MQW system grown by Harman *et al.*[3,4] The main discrepancy comes from the fact that some parameter values used in Broido's work (such as the barrier height for the PbTe quantum well) were not appropriate for describing the specific properties of the samples grown by Harman *et al.*[13] Thus, it has not been possible to make a direct comparison between the theoretical results by Broido *et al.*[12] and the experimental results by Harman *et al.*[3] and Hicks *et al.*[4]

In the present work, we address the issue why the thermoelectric power in *n*-type (111)-oriented PbTe/$Pb_{1-x}Eu_xTe$ MQWs is enhanced in spite of the lifting of the conduction band valley degeneracy in this system. Specifically, we perform a detailed theoretical investigation of the Seebeck coefficient (thermoelectric power) in Pb/$Pb_{1-x}Eu_xTe$ MQWs using the most appropriate as well as the most updated band parameters and carrier concentrations to describe the properties of sample T-225 in Ref. 3, so that a direct comparison can be made with the experimental studies. For example, the Eu content for sample T-225 in Ref. 3 ($x \simeq 0.073$) is now updated to a new value $x \simeq 0.09$ according to the most recent data for the lattice constant as a function of x for $Pb_{1-x}Eu_xTe$ alloys[25] and the x-ray data for sample T-225. Other improvements in our models over the ones by Broido and Reinecke include consideration of the effects of the nonparabolicity for the energy bands and of the anisotropic constant energy surfaces. The effect of the anisotropic constant

energy surface is taken into account by retaining up to the second order term in the Legendre polynomial expansion of the perturbation function $\phi(\mathbf{k})$ as we will discuss in the text. It should be noted that all the parameters used in this study are readily available in the literature in terms of the band parameters for bulk PbTe (Ref. 21) or $Pb_{1-x}Eu_xTe$ alloys.[22–24] Thus, our theoretical analysis requires virtually no fitting parameters, except that the number of carriers in the sample has to be determined by an independent experimental technique such as a Hall coefficient measurement.[6] We believe that such investigations should be of great value not only for acquiring a firm understanding of the physics of the low-dimensional transport phenomena, but also for developing an innovative strategy for designing even better thermoelectric materials in the future using low-dimensional structures.

II. THEORY

A. Solution of Boltzmann equation

The nonequilibrium distribution function for electrons in an electric field $\mathbf{E}$ is obtained by solving the Boltzmann equation

$$\frac{\partial f(\mathbf{k})}{\partial t} = -\frac{e\mathbf{E}}{\hbar}\nabla_{\mathbf{k}} f(\mathbf{k}) + \partial_c f(\mathbf{k}) = 0, \tag{1}$$

where e is the electron charge, $\hbar$ is the Planck constant divided by 2π, $\mathbf{k}$ is the electron wave vector, $f(\mathbf{k})$ is the nonequilibrium electron distribution function, and $\partial_c f(\mathbf{k})$ is the collision term defined by

$$\partial_c f(\mathbf{k}) = -\left(\frac{V_c}{8\pi^3}\right)\int [f(\mathbf{k})\{1-f(\mathbf{k}')\}S(\mathbf{k},\mathbf{k}') - f(\mathbf{k}')\{1-f(\mathbf{k})\}S(\mathbf{k}',\mathbf{k})]\, d\mathbf{k}'. \tag{2}$$

Here, V_c is the sample volume and $S(\mathbf{k},\mathbf{k}')d\mathbf{k}d\mathbf{k}'$ is the scattering probability per unit time that an electron within an infinitesimal volume $d\mathbf{k}$ around $\mathbf{k}$ will be scattered into an infinitesimal volume $d\mathbf{k}'$ around $\mathbf{k}'$ in k space. Since the distribution function $f(\mathbf{k})$ reduces to the Fermi-Dirac distribution function $f_0(E_{\mathbf{k}}) = [1+\exp\{(E_{\mathbf{k}}-\zeta)/k_BT\}]^{-1}$ in the limit of $\mathbf{E}=0$, and $S(\mathbf{k},\mathbf{k}')$ and $S(\mathbf{k}',\mathbf{k})$ have to satisfy the following relation:

$$f_0(E_{\mathbf{k}})\{1-f_0(E_{\mathbf{k}'})\}S(\mathbf{k},\mathbf{k}') - f_0(E_{\mathbf{k}'})\{1-f_0(E_{\mathbf{k}})\}S(\mathbf{k}',\mathbf{k}) = 0, \tag{3}$$

which will be used to express $S(\mathbf{k}',\mathbf{k})$ in terms of $S(\mathbf{k},\mathbf{k}')$. For the case of a two-dimensional electron gas which we will consider in the present work, we substitute $A/4\pi^2$ for the factor $V_c/8\pi^3$ in Eq. (2), where A is the area of the sample, and the integration is carried out over two-dimensional k space.

B. Scattering probability

The scattering probability per unit time $S(\mathbf{k},\mathbf{k}')$ is given by the Fermi golden rule

$$S(\mathbf{k},\mathbf{k}') = \frac{2\pi}{\hbar}|\langle\mathbf{k}'|H'|\mathbf{k}\rangle|^2\,\delta(E_{\mathbf{k}'} - E_{\mathbf{k}} \mp \hbar\omega), \tag{4}$$

where ω is the phonon frequency and the plus and minus signs in the δ function stand for the phonon emission and absorption processes, respectively. The explicit expressions for the squared matrix element $|\langle\mathbf{k}'|H'|\mathbf{k}\rangle|^2$ for the case of a three-dimensional isotropic crystal are given elsewhere for various scattering mechanisms.[26–28]

In the present work, we consider the scattering of the two-dimensionally confined electrons due to the three-dimensional phonons to model the transport coefficients for the two-dimensionally confined electron gas.[12] We note that a state for a two-dimensionally confined electron can be specified by an in-plane wave vector $\mathbf{k}_\parallel$, whereas a state for a phonon is specified by a three-dimensional phonon wave vector $\mathbf{q}$, which will be decomposed into an in-plane component $\mathbf{q}_\parallel$ and a perpendicular component q_z for our convenience in carrying out the calculation. The scattering mechanisms explicitly considered in the present work are (1) longitudinal acoustic phonon deformation potential scattering (LADP) and (2) polar optical phonon scattering (POP). These are the two main scattering mechanisms dominant in bulk PbTe from relatively low ($\sim$77 K) to relatively high temperatures ($>$400 K).[21]

Assuming that the overlap integral for the lattice part of the Bloch function is equal to unity (plane wave approximation), the squared scattering matrix elements for the two-dimensionally confined electrons due to the above mentioned scattering mechanisms are expressed as[27]

$$|\langle\mathbf{k}'_\parallel|H'_{ac}|\mathbf{k}_\parallel\rangle|^2 = \frac{\hbar\Xi^2 k_BT}{4\pi\rho\upsilon^2 A}\int_{-\infty}^{\infty}|G(q_z)|^2 dq_z\,\delta(\mathbf{k}'_\parallel - \mathbf{k}_\parallel \mp \mathbf{q}_\parallel) \tag{5}$$

for the LADP mechanism and

$$|\langle\mathbf{k}'_\parallel|H'_{op}|\mathbf{k}_\parallel\rangle|^2 = \frac{e^2\hbar\omega_0}{4\pi A}\left(\frac{1}{\epsilon_\infty}-\frac{1}{\epsilon_S}\right)\int_{-\infty}^{\infty}\frac{|G(q_z)|^2 dq_z}{|\mathbf{q}_\parallel|^2+q_z^2} \times\left[n(\omega_0)+\frac{1}{2}\mp\frac{1}{2}\right]\delta(\mathbf{k}'_\parallel - \mathbf{k}_\parallel \mp \mathbf{q}_\parallel) \tag{6}$$

for the POP mechanism where $\Xi, \rho, \upsilon, \epsilon_\infty, \epsilon_S, \omega_0$, and $n(\omega_0)$ are, respectively, the acoustic phonon deformation potential, the density of the sample, the speed of sound, the high frequency dielectric constant, the static dielectric constant, the optical phonon frequency, and the occupation number $n(\omega_0) = [\exp(\hbar\omega_0/k_BT)-1]^{-1}$ for phonons with frequency ω_0. Here $G(q_z)$ is defined by

$$G(q_z) = \int_{-\infty}^{\infty}\psi_z^*(z)e^{iq_zz}\psi_z(z)dz, \tag{7}$$

where $\psi_z(z)$ is the normalized wave function in the confinement direction (z direction) that is obtained by solving the Schrödinger equation for a square well potential. It is noted that the elastic approximation ($E_{\mathbf{k}} = E_{\mathbf{k}'}$) and the high temperature approximation for the number of phonons $n(\omega) \simeq k_BT/\hbar\omega$ are used to describe the acoustic phonon scatter-

ing [see Eq. 5]. However, the full inelastic scattering scheme is utilized to describe the optical phonon scattering, as is discussed in the next section.

C. Thermoelectric power

Once the nonequilibrium distribution function $f(\mathbf{k})$ is obtained by solving the Boltzmann equation, the Seebeck coefficient S (thermoelectric power) is readily calculated using the following equations:[26]

$$S=\frac{1}{eT}\frac{\mathbf{L}_{2\mathrm{D}}^{(1)}}{\mathbf{L}_{2\mathrm{D}}^{(0)}}, \tag{8}$$

and

$$\mathbf{L}_{2\mathrm{D}}^{(\alpha)}=e\int\frac{d\mathbf{k}_{\|}}{2\pi^2}f(\mathbf{k}_{\|})\mathbf{v}(\mathbf{k}_{\|})\{E(\mathbf{k}_{\|})-\zeta\}^{\alpha}, \tag{9}$$

where $\mathbf{v}(\mathbf{k}_{\|})$ and $E(\mathbf{k}_{\|})$ are, respectively, the velocity and the energy of the electron in a state $\mathbf{k}_{\|}$, and $\alpha=0,1$. For a multiple subband system such as the PbTe/$Pb_{1-x}Eu_xTe$ MQWs, the transport tensors $\mathbf{L}_{2\mathrm{D}}^{(\alpha)}$s for $\alpha=0,\ 1$ are calculated for each subband separately, and the results are summed together for substitution in Eq. (8) to obtain S for the whole system.

III. CALCULATION

A. Model system

The model system for the present calculation is the (111) oriented PbTe/$Pb_{1-x}Eu_xTe$ multiple quantum wells where $x\simeq 0.09$ and the thicknesses of PbTe and $Pb_{1-x}Eu_xTe$ layers are $\simeq$ 20 and $\simeq$400 Å, respectively (sample T-225 in Ref. 3). The details of the experimental results, including the sample structure, growth conditions, and various transport measurements for this sample are published elsewhere.[3,4] Briefly, it is known that PbTe layers (band gap $E_g=320$ meV at 300 K) serve as the quantum well layers and $Pb_{1-x}Eu_xTe$ layers serve as the barrier layers ($E_g\simeq 600$ meV at 300 K), which results in a conduction band offset of $\simeq 160$ meV. It has been shown experimentally that samples with this structure have a large intrinsic carrier mobility μ and exhibit an enhanced thermoelectric power relative to that for bulk PbTe with a similar carrier concentration.[3,4]

All the band parameters necessary for the numerical calculation of the transport coefficients of the PbTe quantum wells are readily available in the literature.[21–24] In particular, the following values are used in the present calculation from Ref. 12: the anisotropic effective masses at 300 K, $m_t=0.034m$ (transverse component) and $m_l=0.35m$ (longitudinal component), $\hbar\omega_0=14$ meV, $\epsilon_S=33\,\epsilon_0$, and $\epsilon_\infty=414\,\epsilon_0$, where ϵ_0 is the dielectric constant of the vacuum, $\Xi=25$ eV, and $\rho v^2=486$ meV/Å^3. To account for the temperature dependent properties described in the present paper, the temperature dependences of the bulk effective masses and band gap energy are obtained from Refs. 21 and 24, respectively.

The bound state levels for the quantum well are calculated by solving the Schrödinger equation for a square well potential using the empirical relation $\Delta E_c/\Delta E_g=0.55$ where ΔE_c is the conduction band offset and ΔE_g is the difference in band energy gap between $Pb_{1-x}Eu_xTe$ and PbTe.[23] The nonparabolicity of the energy dispersion relation for the confined electronic states is taken into account using the form $\hbar^2k^2/2m^*=E(1+\tilde{\alpha}E)\equiv\gamma(E)$,[26] where E is the electron energy and $\tilde{\alpha}$ is the inverse of E_g. The value of E_g used in our calculation for the ith subband is the energy between the valence- and conduction-band bound state levels for the pertinent subband, denoted by $E_g^{l\text{-}l}$ and $E_g^{o\text{-}o}$ for the longitudinal (l) subband and the oblique (o) subband, respectively.

B. Chemical potential

The chemical potential ζ for the model system is determined by considering the conservation of the total number of carriers per superlattice period $(a+b)$,[6]

$$n_{\mathrm{tot}}\equiv n_{\mathrm{QW}}-p_{\mathrm{QW}}+(n_B-p_B)\frac{b}{a}, \tag{10}$$

where n_{tot} is the apparent total carrier density per quantum well defined by Eq. (10), $n_{\mathrm{QW}}(p_{\mathrm{QW}})$ and $n_B(p_B)$ are the concentrations of electrons (holes) bound to the quantum wells and those delocalized throughout the barrier layer unbound to the quantum wells, respectively. It should be noted that the carrier densities n_{QW} and p_{QW} are calculated using the quantum well thickness (denoted as a), whereas n_B and p_B are calculated using the barrier layer thickness (denoted as b), and hence the factor b/a in Eq. (10). We further note that the carrier densities n_{QW} and p_{QW} have contributions from both the longitudinal valley and the oblique valleys that originate from the four L point valleys in the Brillouin zone for bulk PbTe, and that the carrier density n_B is associated with the L point carriers in the conduction band of the $Pb_{1-x}Eu_xTe$ barrier layer and p_B is associated with the L and Σ point carriers in the valence band of the $Pb_{1-x}Eu_xTe$ barrier layer. In our model system, p_{QW} and p_B are found to be negligible relative to the other terms up to 400 K.[6] Above 400 K the p_B term becomes important due to the large density of states mass ($m_d^*\simeq 1.4$) for the Σ valence band.[21] It was also shown previously that the carrier mobility for the $Pb_{1-x}Eu_xTe$ alloy is greatly reduced relative to that for PbTe,[3] and therefore, in the present work, we assume that the electrical conduction in our model system is entirely due to the carriers that are bound to the quantum wells.

C. Numerical calculation

Once the chemical potential is determined for our model system, the iterative algorithm is employed for the numerical calculation of the nonequilibrium distribution function $f(\mathbf{k}_{\|})$.[26] Taking the x axis as the direction of the electric field that is parallel to one of the principal axes of the 2D elliptical constant energy surface and defining the normalized k vector $\mathbf{k}_{\|}^*$ and the normalized electric field $\mathbf{E}^*$ by $\mathbf{k}_{\|}^*=(k_{\|x}^*,k_{\|y}^*)=(m/m_x k_{\|x},m/m_y k_{\|y})$ and $E_x^*=(m_x/m)E_x$, respectively, we expand $f(\mathbf{k}_{\|})$ as

$$f(\mathbf{k}_{\|})=f_0(E_{\mathbf{k}_{\|}})-\frac{e\hbar E_x^*k_{\|}^*}{m}\left(\frac{\partial f_0}{\partial E}\right)_{E=E_k}\phi(\mathbf{k}_{\|}), \tag{11}$$

where $\phi(\mathbf{k}_\parallel)$ is a perturbation function connected with the application of an electric field and $\phi(\mathbf{k}_\parallel)$ has the units of time. Using the perturbation function $\phi(\mathbf{k}_\parallel)$ in Eq. (11), the Boltzmann equation [Eq. (1)] is rewritten as

$$\cos\theta = \frac{A}{4\pi}\gamma'(E_{\mathbf{k}\parallel})\int \frac{1-f_0(E_{\mathbf{k}'})}{1-f_0(E_{\mathbf{k}})} S(\mathbf{k}_\parallel,\mathbf{k}'_\parallel) \times\{\phi(\mathbf{k}_\parallel)-k^{*\prime}_\parallel/k^*_\parallel\,\phi(\mathbf{k}'_\parallel)\}\,d\mathbf{k}_\parallel, \tag{12}$$

where $\gamma'(E)=d\gamma(E)/dE$, θ is the angle between the vector $\mathbf{k}^*_\parallel$ and the x axis, and Eq. (3) is used to eliminate $S(\mathbf{k}'_\parallel,\mathbf{k}_\parallel)$ in terms of $S(\mathbf{k}_\parallel,\mathbf{k}'_\parallel)$. In solving the Boltzmann equation, the perturbation function $\phi(\mathbf{k}_\parallel)$ is further expanded using the Legendre polynomials $P_l(x)$ and the two most significant terms, i.e., $\phi(\mathbf{k}_\parallel)=a_1(E)P_1(\cos\theta)+a_3(E)P_3(\cos\theta)$, are retained in the iteration procedure. The resultant Boltzmann equation is solved for $a_1(E)$ and $a_3(E)$. The reason that we retain the second term in the expansion of $\phi(\mathbf{k}_\parallel)$ is to handle the anisotropy of the constant energy surface for the oblique valley accurately in solving the Boltzmann equation. In this way, we were able to keep the error associated with the numerical calculations to within a few percent. To complete our calculation for the oblique valleys, the procedure above is repeated for $\mathbf{E}^*$ parallel to the y axis and the transport coefficients calculated along the x and y axes are averaged to yield the final isotropic transport coefficient that is consistent with the cubic symmetry of the model system.[26]

IV. RESULTS

A. Constant relaxation time approximation

The enhanced Seebeck coefficient observed in the (111)-oriented $PbTe/Pb_{1-x}Eu_xTe$ MQWs was previously explained qualitatively using the constant relaxation time approximation (CRTA) and the two-band model assuming parabolic energy bands:[4,6] the total Seebeck coefficient S is given by $(\sigma_1S_1+\sigma_2S_2)/(\sigma_1+\sigma_2)$ where σ_i and S_i $(i=1,2)$ are the electrical conductivity and the Seebeck coefficient, respectively, for the ith subband. For the (111)-oriented $PbTe/Pb_{1-x}Eu_xTe$ MQWs, four equivalent L point minima in the 3D Brillouin zone split into one longitudinal (lowest in energy) and three equivalent oblique pockets in 2D quantum wells; thus, we associate the longitudinal and the oblique subbands with the first and second subbands in the abovementioned two-band model.

Since the carrier concentration and the Seebeck coefficient of a single band material are functions of only the chemical potential and temperature, for a given band structure in the CRTA, we need only one additional parameter when we extend the single subband model to the two-band model in calculating the total S. This additional parameter is the ratio of the carrier mobilities μ (or scattering times τ) between these subbands, namely, $\mu_{\text{obliq}}/\mu_{\text{longt}}=(\tau_{\text{obliq}}/m_{\text{obliq}})/(\tau_{\text{longt}}/m_{\text{longt}})\simeq 0.553\tau_{\text{obliq}}/\tau_{\text{longt}}$ where $m_{\text{longt}}=m_{\parallel t}$ and $m_{\text{obliq}}=2/(m_{\parallel t}^{-1}+m_{\parallel l}^{-1})$ are the transport masses for the longitudinal subband and oblique subband, respectively. The experimental results for the Seebeck coefficient as a function of Hall carrier concentration are shown in Fig. 1 for bulk PbTe and $PbTe/Pb_{1-x}Eu_xTe$ MQWs from Ref. 3 together with the theoretical results obtained using the CRTA with three different assumptions for the mobility ratio.[6] The assumptions used in the CRTA in Fig. 1 are obtained for various situations of the intravalley and the intervalley scattering, assuming that the relaxation time τ is inversely proportional to the density of states for electrons (see Ref. 6 for details). We should, however, note that the observed enhancement in S can be understood, without including intervalley scattering, as we discuss in the following sections. Therefore, in this section, we simply restate that the simple density of states consideration for τ, assuming only intravalley scattering ($\tau_{\text{obliq}}=0.33\tau_{\text{longt}}$), leads to S values for MQWs as small as that for PbTe bulk, and does not explain the enhancement in S observed experimentally.

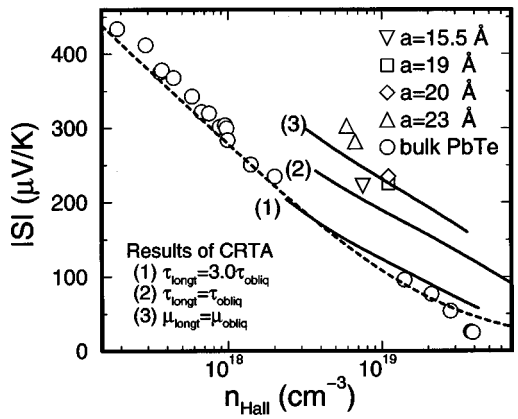

FIG. 1. The absolute value of the measured Seebeck coefficient as a function of Hall carrier concentration for bulk PbTe (open circles) and for $PbTe/Pb_{1-x}Eu_xTe$ MQWs of various quantum well thicknesses (other open symbols) at 300 K. The theoretical result for $|S|$ for bulk PbTe using the constant relaxation time approximation (CRTA) and using values of $m_t=0.034m$ and $m_l=0.35m$ for the bulk effective masses is shown by the dashed curve. The theoretical results for $PbTe/Pb_{1-x}Eu_xTe$ MQWs in the CRTA are shown for the following conditions (see Ref. 6 for the meaning of these conditions): (1) $\tau_{\text{longt}}=3\tau_{\text{obliq}}$, (2) $\tau_{\text{longt}}=\tau_{\text{obliq}}$, and (3) $\mu_{\text{longt}}=\mu_{\text{obliq}}$.

The experimental results for the Seebeck coefficient as a function of temperature for sample T-225 in Ref. 3 are plotted in Fig. 2 together with the theoretical results using the CRTA, assuming the $\mu_{\text{obliq}}=\mu_{\text{longt}}$ and $\tau_{\text{obliq}}=\tau_{\text{longt}}$ conditions.[7] In the theoretical calculation, $n_{\text{tot}}=1.1\times10^{19}$ cm^{-3} is assumed, based on the previous analysis of the Hall coefficient measurements as a function of temperature.[6] We note that although the results for the CRTA with the conditions $\mu_{\text{obliq}}=\mu_{\text{longt}}$ and $\tau_{\text{obliq}}=\tau_{\text{longt}}$ are consistent with the experiment at certain specific temperatures, there is no *a priori* reason that either the $\mu_{\text{obliq}}=\mu_{\text{longt}}$ or the $\tau_{\text{obliq}}=\tau_{\text{longt}}$ conditions should hold at any particular temperature. More importantly, the fitting of the experimental results, obtained from the two-band model using the CRTA, suggests that the reduction of the Seebeck coefficient due to the lifting of the valley degeneracy becomes less significant as the temperature is increased. Therefore, it is of interest to investigate the detailed mechanisms that are responsible for the observed enhancement in the Seebeck coefficient for the $PbTe/Pb_{1-x}Eu_xTe$ MQWs relative to that for the corresponding bulk PbTe. Such an investigation

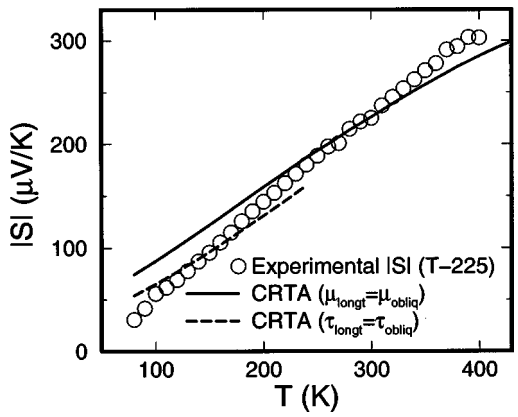

FIG. 2. Absolute value of the Seebeck coefficient for the $PbTe/Pb_{1-x}Eu_xTe$ MQW sample (T-225) as a function of temperature (open circles). The solid line shows the theoretical results using the CRTA assuming $\mu_{\rm longt}=\mu_{\rm obliq}$, whereas the dashed line shows the results assuming $\tau_{\rm longt}=\tau_{\rm obliq}$.

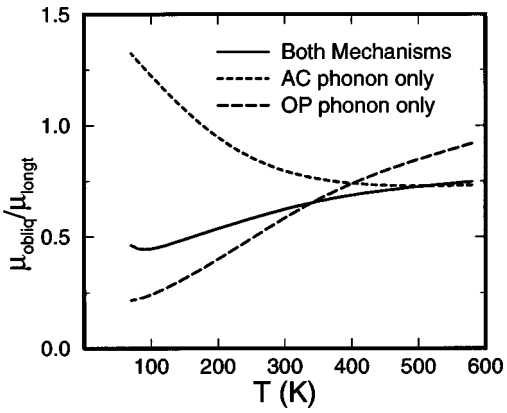

FIG. 3. Calculated values for the mobility ratio between the carriers in the oblique valley and in the longitudinal valley in (111)-oriented $PbTe/Pb_{1-x}Eu_xTe$ MQWs when (1) only the longitudinal acoustic phonon deformation potential scattering (LADP) is considered (short-dashed curve), (2) only the polar optic phonon scattering (POP) is considered (long-dashed curve), and (3) both LADP and POP are considered (solid curve).

should be important not only to understand the fundamental physics of the low-dimensional transport phenomena, but also to employ the ideas gained through the investigation of such mechanisms to design even better thermoelectric materials in the future. In the next section, we address these points in more detail by comparing the experimental results for sample T-225 with our theoretical results, first assuming longitudinal acoustic phonon deformation potential scattering and polar optical phonon scattering independently, and then considering both mechanisms acting together.

B. Seebeck coefficient due to acoustic phonon scattering

Using the elastic and high temperature approximations described in the previous section and considering only the longitudinal acoustic phonon deformation potential scattering, the Boltzmann equation [Eq. (12)] reduces to the energy-dependent relaxation time $\tau_{ac}(E)$ approximation:

$$\tau_{ac}(E)^{-1}\equiv a_1(E)^{-1} = \frac{(m_x m_y)^{1/2}}{4\pi\hbar^3}\frac{\Xi^2 k_B T}{\rho v^2}\gamma'(E)^2\int |G(q_z)|^2 dq_z\times 2, \tag{13}$$

where the factor 2 at the end of the equation accounts for the phonon absorption and emission processes. Using Eq. (13), we can directly investigate the ratio of τ_{ac} between the oblique subbands (denoted by $\tau_{ac}^{\rm obliq}$) and the longitudinal subband (denoted by $\tau_{ac}^{\rm longt}$) for our model system.

If the energy dispersion relation is completely parabolic, the relaxation time τ_{ac} is constant with energy, so that the energy dependent τ formalism basically reduces to the CRTA. In this limit, τ_{ac} is proportional to the product of the density-of-states mass $(m_x m_y)^{1/2}$ and the $|G(q_z)|^2$ integral as seen in Eq. (13). Using the bulk effective masses at 300 K projected onto the plane of the quantum well, we obtain $m_x = m_y \equiv m_{\|t}=0.034m$ for the longitudinal pocket and $m_x \equiv m_{\|l}=0.315m$, $m_y\equiv m_{\|t}=0.034m$ for each of the oblique pockets. Therefore, the difference in the effective masses accounts for a factor of 0.33 in $\tau_{ac}^{\rm obliq}/\tau_{ac}^{\rm longt}$. Another factor comes from the $|G(q_z)|^2$ integral. Since the z component of the electron wave function for the longitudinal subband is more confined than that for the oblique subband, the resultant $G(q_z)$, and hence also the $|G(q_z)|^2$ integral, is larger for the longitudinal subband than for the oblique subband. This factor accounts for a factor of 3.77 in $\tau_{ac}^{\rm obliq}/\tau_{ac}^{\rm longt}$ at 300 K. Therefore the value for $\tau_{ac}^{\rm obliq}/\tau_{ac}^{\rm longt}$ assuming a parabolic energy dispersion relation is $0.33\times 3.77=1.26$, which is quite different from the naive assumption $\tau^{\rm obliq}/\tau^{\rm longt}=0.33$ obtained from the density of states factor only. Furthermore, when using a nonparabolic energy dispersion relation, we have an additional factor of $\gamma'(E)^2$ in Eq. (13) where $E=\zeta$ (where ζ is the chemical potential) for the longitudinal subband. For our model system at 300 K we find that the Fermi level is 30.15 meV above the longitudinal subband edge and 42.48 meV below the oblique subband edge, where the energy band gaps between the valence and conduction band bound states are 447.69 meV for the longitudinal subband ($E_g^{l\text{-}l}$) and 581.87 meV for the oblique subband ($E_g^{o\text{-}o}$). Since the Fermi energy lies at a degenerate energy (inside the band) only with the longitudinal subband, the additional contribution of the nonparabolicity of the energy bands to $\tau_{ac}^{\rm obliq}/\tau_{ac}^{\rm longt}$ becomes important only for the longitudinal subband. For $\zeta=30.15$ meV and $E_g^{l\text{-}l}=447.69$ meV, we obtain $\gamma'(\zeta)^2=1.29$ at 300 K. It turns out that the contribution of the nonparabolicity to $\tau_{ac}^{\rm obliq}/\tau_{ac}^{\rm longt}$ is strongly dependent on temperature. For example at 100 K, we find that the Fermi level is 90.6 meV above the longitudinal subband edge and $E_g^{l\text{-}l}$ is 382.93 meV, and therefore we get $\gamma'(\zeta)^2=2.17$. From this argument, we find that the temperature dependence of $\tau_{ac}^{\rm obliq}/\tau_{ac}^{\rm longt}$ mainly comes from the effect of the nonparabolicity of the energy bands (see Fig. 3).

Shown in Fig. 4 are the experimental Seebeck coefficient ($S_{\rm exp}$, open circles) as well as the theoretical Seebeck coefficients: (1) considering only longitudinal acoustic phonon deformation potential scattering ($S_{\rm ac}$, short-dashed curve) and (2) considering only polar optical phonon scattering ($S_{\rm op}$, long-dashed curve). One can see that $S_{\rm ac}$ is smaller

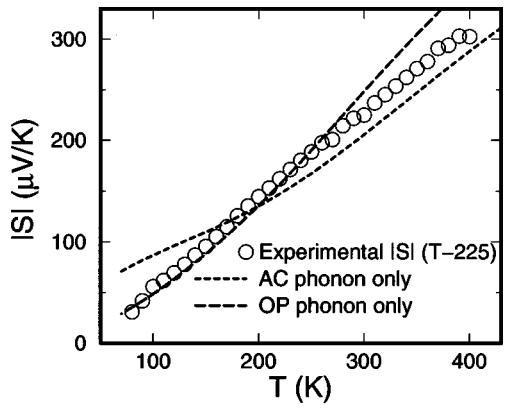

FIG. 4. Absolute value of the Seebeck coefficient for the $PbTe/Pb_{1-x}Eu_xTe$ MQW sample (T-225) as a function of temperature (open circles) together with the theoretical results (1) considering only the longitudinal acoustic phonon deformation potential (short-dashed curve) and (2) considering only the polar optic phonon scattering (long-dashed curve).

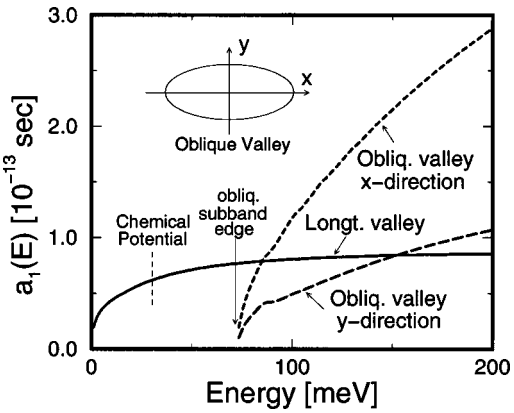

FIG. 5. The coefficient $a_1(E)$ for the first order term in the Legendre polynomial expansion of the perturbation function $\phi(\mathbf{k}_\parallel)$ as a function of energy (see text). The solid, short-dashed, and long-dashed curves denote the functions determined for $a_1(E)$ for the longitudinal valley, the oblique valley along the x direction, and the oblique valley along the y direction, respectively. Also indicated on the figure are the energy values for the chemical potential and the oblique subband edge.

than S_{exp} above 200 K, while it is larger than S_{exp} below 150 K. The main reason for the large S_{exp} compared with S_{ac} above 200 K is that the polar optical phonon scattering generally has an effect to increase the value of S as we will discuss in the next section. This effect is predominant above 200 K. On the other hand, at lower temperatures ($\leqslant$150 K), the $\gamma(\zeta)^2$ factor in Eq. (13) increases for the longitudinal subband, causing $\tau_{\text{ac}}^{\text{longt}}$ to decrease. Hence S_{ac} increases, while in the real sample the polar optical phonons contribute to the preferential scattering of the carriers in the oblique valleys while leaving the scattering of the carriers in the longitudinal valley relatively unchanged. This is the mechanism which explains the reduced S_{exp} relative to S_{ac} at low temperatures ($\leqslant$150 K).

C. Seebeck coefficient due to optical phonon scattering

The Seebeck coefficient S calculated considering the polar optical phonon scattering only (denoted by S_{op}) is also shown in Fig. 4 (long-dashed curve) as a function of temperature. The calculated ratio of the mobilities $\mu_{\text{obliq}}/\mu_{\text{longt}}$ when only the polar optical phonon scattering is considered [denoted by $(\mu_{\text{obliq}}/\mu_{\text{longt}})_{\text{POP}}$] is also plotted as a function of temperature in Fig. 3 (long-dashed curve). We find that $(\mu_{\text{obliq}}/\mu_{\text{longt}})_{\text{POP}}$ is also a strong function of temperature and this ratio becomes as small as 0.25 below 100 K. This observation proves the postulate in the previous section that the polar optical phonons are more effective in scattering carriers in the oblique valleys than scattering carriers in the longitudinal valley at low temperatures in our model system. Another observation is that although the value for $(\mu_{\text{obliq}}/\mu_{\text{longt}})_{\text{POP}}$ is 0.6$\sim$0.9 for temperatures above 300 K (i.e., $\mu_{\text{obliq}}<\mu_{\text{longt}}$), whereas we find that $\mu_{\text{obliq}}\geqslant\mu_{\text{longt}}$ is consistent with the experimental result in the CRTA, the resulting S_{op} calculated for our model system is significantly greater than S_{exp} above 300 K. This apparent discrepancy is resolved if we look at the special shape of the distribution function $f(E)$. Plotted in Fig. 5 is the coefficient for the first order term, $a_1(E)$, of the perturbation function $\phi(\mathbf{k})$ as a function of energy. Since $a_1(E)$ (which is interpreted as the scattering time τ in a naive sense) increases with increasing energy near the band edge, we can expect S_{op} to become significantly larger than S_{exp} if the chemical potential ζ is near (or below) the band edge and the width of the rising edge of the $a_1(E)$ function is larger than the magnitude of the thermal energy k_BT.

D. Seebeck coefficient due to both the longitudinal acoustic phonons and the polar optical phonons

When we consider both longitudinal acoustic phonon deformation potential (LADP) scattering and polar optical phonon (POP) scattering, and we then calculate the Seebeck coefficient for both of these scattering mechanisms acting at the same time (S_{tot}), we simply add the contributions from these scattering mechanisms to obtain the total scattering probability per unit time [Eq. (4)] and use the same iterative approach described in the previous section. The resulting S_{tot} calculated in this way is plotted as a function of temperature

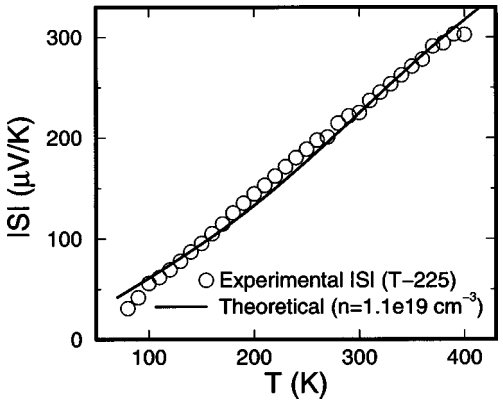

FIG. 6. Absolute value of the Seebeck coefficient for the $PbTe/Pb_{1-x}Eu_xTe$ MQW sample (T-225) as a function of temperature (open circles) together with the theoretical results obtained for $|S|$, considering both longitudinal acoustic phonon deformation potential scattering and polar optical phonon scattering (solid curve).

in Fig. 6 (solid curve) together with the experimental results (S_{exp}, open circles). We note that the agreement in Fig. 6 between the theoretical and experimental results is fairly good for the wide temperature range from 80 to 400 K based on literature values for the band parameters and no adjustable parameters that are fitted by the model. The good agreement between the theoretical and experimental results indicates the reliability of the parameters deduced from the previous measurements[3] and analyses,[6] such as carrier concentrations, lattice constants and band energy gaps, and the validity of the basic idea proposed by Hicks and Dresselhaus[1,16] which predicts enhanced thermoelectric properties for low-dimensional systems, if the original model calculation is properly refined to include the appropriate scattering mechanisms.

V. CONCLUSIONS

A theoretical investigation has been performed to reveal the mechanism of the observed enhanced thermoelectric power S in (111)-oriented $PbTe/Pb_{1-x}Eu_xTe$ multiple-quantum-wells. This enhancement in S occurs in spite of the lifting of the valley degeneracy between the longitudinal and oblique valleys at the L point in the Brillouin zone, which would tend to reduce S. We have considered the effects of longitudinal acoustic phonon deformation potential scattering and the effects of polar optical phonon scattering on the two-dimensionally confined electrons in the quantum wells. In the low temperature regime (~ 100 K), we find that polar optical phonons are more effective in scattering the carriers in the oblique valleys than in scattering carriers in the longitudinal valley. Since the occupation of the oblique valleys is small at low T, the resulting thermoelectric power is relatively small. However, in the high temperature regime ($\simeq 300$ K), where there is more occupation of the oblique valleys, polar optical phonon scattering is found to contribute to increasing S because of the particular shape of the distribution function created by polar optical phonon scattering. Our theoretical result for the two scattering mechanisms acting together yields good agreement with the experimental results over a wide temperature range (80–400 K) without the use of any fitting parameters. It is hoped that the knowledge acquired through this study will contribute to deepening our understanding of the fundamental physics of low-dimensional transport phenomena, as well as to allowing us to plan a new strategy for designing useful thermoelectric materials using low-dimensional structures in the future.

ACKNOWLEDGMENTS

The authors would like to thank Dr. D. A. Broido at Boston College and Dr. T. L. Reinecke at the Naval Research Laboratory for valuable discussions and for advice regarding the numerical calculations made in this work. The authors are also thankful to Dr. G. Springholz and Professor G. Bauer at the Johannes Kepler Universität, Linz, Austria, for providing us with the supplemental PbTe MQW samples to study μ_{obliq}/μ_{longt} as a function of carrier concentrations and temperature, and to Dr. G. Dresselhaus at MIT and Professor H. Ehrenreich at Harvard University for valuable discussions and inputs. Support from the U.S. Navy (Grant No. N00167-98-K-0024) for this work is gratefully acknowledged. The Lincoln Laboratory portion of this work was sponsored by the Department of the Navy, the Army Research Office, and the Defense Advanced Research Projects Agency (DARPA) under AF Contract No. F19628-95-0002.

[1] L.D. Hicks and M.S. Dresselhaus, Phys. Rev. B **47**, 12 727 (1993).
[2] L.D. Hicks, T.C. Harman, and M.S. Dresselhaus, Appl. Phys. Lett. **63**, 3230 (1993).
[3] T.C. Harman, D.L. Spears, and M.J. Manfra, J. Electron. Mater. **25**, 1121 (1996).
[4] L.D. Hicks, T.C. Harman, X. Sun, and M.S. Dresselhaus, Phys. Rev. B **53**, R10 493 (1996).
[5] T.C. Harman, D.L. Spears, D.R. Calawa, S.H. Groves, and M.P. Walsh, *Proceedings of the XVI International Conference on Thermoelectrics, Dresden, Germany, 1997* (IEEE, Piscataway, NJ, 1997).
[6] T. Koga, S.B. Cronin, T.C. Harman, X. Sun, and M.S. Dresselhaus, in *Semiconductor Process and Device Performace Modeling*, MRS Symposia No. 490, edited by J.S. Nelson *et al.* (MRS, Pittsburgh, 1998), p. 263.
[7] T. Koga, S. B. Cronin, T. C. Harman, X. Sun, and M. S. Dresselhaus (unpublished).
[8] J.O. Sofo and G.D. Mahan, Appl. Phys. Lett. **65**, 2690 (1994).
[9] P.J. Lin-Chung and T.L. Reinecke, Phys. Rev. B **51**, 13 244 (1995).
[10] D.A. Broido and T.L. Reinecke, Phys. Rev. B **51**, 13 797 (1995).
[11] D.A. Broido and T.L. Reinecke, Appl. Phys. Lett. **67**, 1170 (1995).
[12] D.A. Broido and T.L. Reinecke, Appl. Phys. Lett. **70**, 2834 (1997).
[13] T. Koga, T.C. Harman, S.B. Cronin, and M.S. Dresselhaus (unpublished).
[14] T. Koga, X. Sun, S.B. Cronin, M.S. Dresselhaus, K.L. Wang, and G. Chen, J. Comput.-Aided Mat. Des. **4**, 175 (1997).
[15] T. Koga, X. Sun, S.B. Cronin, and M.S. Dresselhaus, Appl. Phys. Lett. **73**, 2950 (1998).
[16] L.D. Hicks and M.S. Dresselhaus, Phys. Rev. B **47**, 16 631 (1993).
[17] D.A. Broido and T.L. Reinecke, Appl. Phys. Lett. **67**, 100 (1995).
[18] Z. Zhang, J.Y. Ying, and M.S. Dresselhaus, J. Mater. Res. **13**, 1745 (1998).
[19] Z. Zhang, X. Sun, M.S. Dresselhaus, J.Y. Ying, and J.P. Heremans, Appl. Phys. Lett. **73**, 1589 (1998).
[20] X. Sun, Z. Zhang, and M.S. Dresselhaus, Appl. Phys. Lett. **74**, 4005 (1999).
[21] R. Dornhaus, G. Nimtz, and B. Schlicht, *Narrow-Gap Semiconductors*, Vol. 98 of Springer Tracts in Modern Physics (Springer-Verlag, Berlin, 1985).
[22] S. Yuan, H. Krenn, G. Springholz, and G. Bauer, Phys. Rev. B **47**, 7213 (1993).
[23] S. Yuan, G. Springholz, G. Bauer, and M. Kriechbaum, Phys. Rev. B **49**, 5476 (1994).

[24] S. Yuan, H. Krenn, G. Springholz, Y. Ueta, G. Bauer, and P.J. McCann, Phys. Rev. B **55**, 4607 (1997).
[25] A.Y. Ueta, Ph.D. thesis, the Johannes Kepler Universität Linz, 1997.
[26] B.R. Nag, *Electron Transport in Compound Semiconductors*, Vol. 11 of Springer Series in Solid-State Sciences (Springer-Verlag, Berlin, Heidelberg, 1980).
[27] K. Tomizawa, *Numerical Simulation of Submicron Semiconductor Devices* (Artech House, Inc., Norwood, 1993).
[28] A.K. Das and B.R. Nag, J. Phys. Chem. Solids **39**, 259 (1978).